



**HAL**  
open science

## Surface Engineering of a Mg Electrode via a New Additive to Reduce Overpotential

Zhen Meng, Zhenyou Li, Liping Wang, Thomas Diemant, Dasari Bosubabu, Yushu Tang, Romain Berthelot, Zhirong Zhao-Karger, Maximilian Fichtner

► **To cite this version:**

Zhen Meng, Zhenyou Li, Liping Wang, Thomas Diemant, Dasari Bosubabu, et al.. Surface Engineering of a Mg Electrode via a New Additive to Reduce Overpotential. *ACS Applied Materials & Interfaces*, 2021, 13 (31), pp.37044-37051. 10.1021/acsami.1c07648 . hal-03329675

**HAL Id: hal-03329675**

**<https://hal.science/hal-03329675>**

Submitted on 31 Aug 2021

**HAL** is a multi-disciplinary open access archive for the deposit and dissemination of scientific research documents, whether they are published or not. The documents may come from teaching and research institutions in France or abroad, or from public or private research centers.

L'archive ouverte pluridisciplinaire **HAL**, est destinée au dépôt et à la diffusion de documents scientifiques de niveau recherche, publiés ou non, émanant des établissements d'enseignement et de recherche français ou étrangers, des laboratoires publics ou privés.

# Surface Engineering of Mg Electrode via New Additive to Reduce Overpotential

*Zhen Meng,<sup>†\*</sup> Zhenyou Li,<sup>†</sup> Liping Wang,<sup>†</sup> Thomas Diemant,<sup>†</sup> Dasari Bosubabu,<sup>†</sup>*

*Yushu Tang,<sup>‡</sup> Romain Berthelot,<sup>§,||</sup> Zhirong Zhao-Karger,<sup>†\*</sup> Maximilian Fichtner<sup>†‡\*</sup>*

<sup>†</sup> Helmholtz Institute Ulm (HIU) Electrochemical Energy Storage, Helmholtzstraße 11,  
D-89081 Ulm, Germany

<sup>‡</sup> Institute of Nanotechnology, Karlsruhe Institute of Technology (KIT), Hermann-von  
-Helmholtz-Platz 1, D-76344 Eggenstein-Leopoldshafen, Germany

<sup>§</sup> ICGM, Univ. Montpellier, CNRS, ENSCM, 34095, Montpellier, France

<sup>||</sup> Réseau sur le Stockage Electrochimique de l'Énergie (RS2E), CNRS, 80039,  
Amiens, France

\*Corresponding authors:

E-mail:

zhen.meng@partner.kit.edu (Zhen Meng)

zhirong.zhao-karger@kit.edu (Zhirong Zhao-Karger)

maximilian.fichtner@kit.edu (Maximilian Fichtner)

**ABSTRACT:** In non-aqueous Mg batteries, inactive adsorbed species and the passivation layer formed from the reactive Mg with impurities in the electrolyte seriously affect the Mg metal/electrolyte interface. These adlayers can impede the passage of  $\text{Mg}^{2+}$  ions, leading to high Mg plating/stripping overpotential. Herein, we report the properties of a new additive, bismuth triflate ( $\text{Bi}(\text{OTf})_3$ ), for chlorine-free Mg electrolyte to enhance Mg plating/stripping from initial cycles. The beneficial effect of  $\text{Bi}(\text{OTf})_3$  can be ascribed to the  $\text{Bi}/\text{Mg}_3\text{Bi}_2$  formed *in-situ* on the Mg metal surface, which increases the charge transfer during the on-off transition by reducing the adsorption of inactive species on the Mg surface and enhancing the resistance of the reactive surface to passivation. This simple method provides a new avenue to improve the compatibility between Cl-free Mg electrolyte and Mg metal anode.

**KEYWORDS:** magnesium-bismuth, Mg interface, conditioning free, low overpotential, magnesium battery.

## 1. INTRODUCTION

In recent years, the Mg battery has raised considerable interest due to the virtues of the Mg anode, including the high volumetric energy density ( $3833 \text{ mAh/cm}^3$ ), natural abundance, and low cost.<sup>1-4</sup> To achieve reversible Mg plating/stripping, considerable progress has been made in the field of Mg electrolytes in recent years, where several electrolyte systems with high Mg stripping/plating efficiency have been reported by some research groups.<sup>5-11</sup> In this context, our group developed a non-corrosive  $\text{Mg}[\text{B}(\text{hfp})_4]_2$  (MgBOR) salt electrolyte, which exhibits high compatibility for Mg plating/stripping and enhanced oxidative stability compared with conventional Mg

electrolytes.<sup>12</sup>

Though the pressing issues related to Mg electrolytes have been extensively investigated, some unfavorable phenomena on the Mg anode/electrolyte interface still impede its practical application, including the notorious passivation layer caused by the reduction of Mg salt and/or the impurities (H<sub>2</sub>O, CO<sub>2</sub>, etc.), and the electrochemical inactive adsorbed species on the Mg surface.<sup>13–18</sup> Both of them hinder Mg<sup>2+</sup> ion transfer, resulting in large anode overpotential. The former can even cause a failure of reversible Mg plating/stripping,<sup>13,18</sup> whereas the latter has been identified as a unique phenomenon of the Mg battery, independent of the electrolyte formulation.<sup>18</sup> Preliminary conditioning could activate the Mg/electrolyte interface in some electrolyte systems.<sup>19,20</sup> However, this is time-consuming and expensive. Alternatively, establishing an interphase with less tendency to form such passivation and adsorption layers and conduct Mg<sup>2+</sup> ions is a more straightforward approach. For instance, an artificial SEI for Mg anode has been synthesized from thermal-cyclized polyacrylonitrile and Mg triflate.<sup>21</sup> Iodine has been introduced as a Mg electrolyte additive, which forms a Mg iodide layer on Mg anode to work as the Mg<sup>2+</sup> ion conductive interface.<sup>15</sup>

Recently, some auxiliary metal-based interphase layers were also reported to exhibit much more compatible anode/electrolyte interfaces than the bare Mg anode. Cui *et al.* demonstrated an efficient Li-species-containing SEI for the Mg anode by partial decomposition of LiB(hfip)<sub>4</sub> on the Mg.<sup>22</sup> Very recently, the strategy of using Ge, Sn metals and their compounds to protect Mg anode has been investigated by Luo

*et al.*<sup>23,24</sup> In one case, 0.4 M GeCl<sub>4</sub> was added in 0.5 M Mg(TFSI)<sub>2</sub>/DME electrolyte to form a Ge, GeO<sub>x</sub> protecting layer on the Mg anode.<sup>23</sup> In the other case, SnCl<sub>2</sub>/DME solution was employed to pretreat the Mg surface, resulting in a layer consisting of Sn, Mg<sub>2</sub>Sn, MgCl<sub>2</sub>, and SnCl<sub>2</sub>.<sup>24</sup> Note that the introduced Cl<sup>-</sup> ions could affect the coordination environment of Mg<sup>2+</sup> ions and the interfacial behavior of the Mg anode.<sup>25-28</sup>

In this study, we investigated the feasibility of a bismuth-based surface layer at Mg anode on forming a functional interface. It has been reported that Bi could react with Mg to form Mg<sub>3</sub>Bi<sub>2</sub>, which has high Mg<sup>2+</sup> ion conductivity ( $\sim 10^{-10}$  cm<sup>2</sup> s<sup>-1</sup>) and high resistance to passivation.<sup>29-31</sup> In order to elucidate the function of the interphase solely, we tried to avoid any Cl-containing species in the system by applying bismuth (III) trifluoromethanesulfonate (Bi triflate or Bi(OTf)<sub>3</sub>) as an additive in the Mg[B(hfip)<sub>4</sub>]<sub>2</sub>/DME (MgBOR/DME) electrolyte. The MgBOR/DME electrolyte system displays excellent compatibility with pure Mg anode and performs with a low overpotential. Nevertheless, significantly high plating/stripping overpotential with large initial interfacial impedance was observed in the initial electrochemical cycles. This large impedance could be lowered via an “activation” process, which is believed to be slow and gradual.<sup>18</sup> By adding the Bi(OTf)<sub>3</sub> as an additive into the Cl-free electrolyte, Mg plating/stripping performance was enhanced remarkably during the on-off transition (when the current starts to pass through the electrodes) and the following dozens of cycles. More impressively, this additive-containing electrolyte exhibited high tolerance towards the presence of H<sub>2</sub>O (measured up to 128 ppm).

## 2. EXPERIMENTAL SECTION:

### 2.1. Electrolyte preparation:

Anhydrous 1, 2-dimethoxyethane (DME, 99.5 %, inhibitor-free) was purchased from Sigma-Aldrich and dried with molecular sieves (3 Å, Fisher Chemical). Prior to the electrolyte preparation, Bi(OTf)<sub>3</sub> was dried at 200 °C under vacuum for 10 h.

**Preparation of 0.3M MgBOR/DME:** The electrolyte salt Mg[B(hfip)<sub>4</sub>]<sub>2</sub>·3DME was synthesized by following the previous methods.<sup>12,35</sup> Then, 0.3 M electrolyte solution was prepared by dissolving Mg[B(hfip)<sub>4</sub>]<sub>2</sub>·3DME into an appropriate amount of DME with a volumetric flask.

**Preparation of electrolyte with additive:** Bi(OTf)<sub>3</sub> additive was added into the 0.3M MgBOR /DME electrolyte to prepare the electrolytes with the additive concentration of 2 mM, 10 mM, and 50 mM, respectively

### 2.2. Electrodes preparation:

**Mo<sub>6</sub>S<sub>8</sub> electrode preparation:** Mo<sub>6</sub>S<sub>8</sub> powder (NEI Corporation), conductive carbon C65, and PVDF (Alfa Aesar) binder were mixed with a mass ratio of 7:2:1 in NMP to form a slurry. The slurry was cast onto stainless steel and dried. The diameter of the electrode is 11.8 mm. The loading of Mo<sub>6</sub>S<sub>8</sub> on the electrode is 1.0-1.8 mg cm<sup>-2</sup>.

**Mg-Bi (Bi modified Mg) electrode preparation:** Scratched Mg foil was directly immersed into 200 μL of 10 mM or 100 mM of Bi(OTf)<sub>3</sub>/DME electrolyte for 10s. Afterward, it was washed with DME and used directly as a Mg-Bi electrode.

### 2.3. Electrochemical characterization

In the cyclic voltammetry (CV) tests, Pt foil or stainless steel (316) foil was used as a

working electrode and Mg foil as a counter electrode. The scan rate was  $50 \text{ mV s}^{-1}$ . Electrochemical impedance spectra (EIS) were measured from 1 MHz to 10 mHz. Three-electrode PAT-Cell (from EL-cell) was assembled for  $\text{Mo}_6\text{S}_8/\text{Mg}$  battery tests. The CV, EIS, and 3-electrode tests were performed using a Bio-logic VMP3 potentiostat. Mg or Mg-Bi foils with a diameter of 10 mm were used separately for the two-electrode symmetric cells (Swagelok) with current densities of  $1 \text{ mA cm}^{-2}$  or  $0.1 \text{ mA cm}^{-2}$  for 0.5 h at each step. The electrolyte amounts in two-electrode Swagelok and three-electrode cells were  $50 \text{ }\mu\text{L}$  and  $120 \text{ }\mu\text{L}$ , respectively. The data was recorded using an Arbin battery cycling unit.

#### **2.4. Characterization**

X-ray diffraction (XRD) analysis was conducted with a Bruker D8 advanced XRD diffractometer with a Cu  $K\alpha$  source. Scanning electron microscopy (SEM) and Energy-Dispersive X-ray Spectroscopy (EDX) were performed in a Zeiss LEO 1530 with EDX detector X-maxN from Oxford instruments. XPS measurements were carried out on a Specs XPS system with a Phoibos 150 energy analyzer using monochromatic Al  $K\alpha$  radiation ( $1486.6 \text{ eV}$ ), a take-off angle of  $45^\circ$ , and pass energies of 30 and 90 eV at the analyzer for detail and survey spectra, respectively. The samples were transferred under Ar from the glovebox to the XPS system to avoid contamination. CasaXPS was used for data analysis, using Shirley-type backgrounds and Gaussian-Lorentzian peak shapes. For the Bi4f peak (P2p and S2p), peak doublets with the expected intensity ratio (4:3) and spin-orbit splitting (5.3 eV) were used for the peak fit. All spectra were calibrated to the C (1s) peak of adventitious carbon at

284.8 eV.

### 3. RESULTS AND DISCUSSION

#### 3.1 Effects of Bi(OTf)<sub>3</sub> on Mg Electrochemistry

Cyclic voltammetry studies of the 0.3M MgBOR/DME electrolyte with and without 10 mM Bi(OTf)<sub>3</sub> as additive were carried out in two-electrode cells with stainless steel as working electrode, and results are given in **Figure 1**. Using the blank electrolyte (0.3 M MgBOR/DME), the first cathodic scan displays the reductive current associated with Mg plating starting at  $-0.50$  V and oxidative current associated with Mg stripping at  $0.20$  V. Only a small reductive peak current of  $3 \text{ mA cm}^{-2}$  was detected. A continuously increasing reductive peak current was observed in the following cycles (**Figure 1b**), which eventually stabilized at  $55 \text{ mA cm}^{-2}$  after 14 cycles. An analogous phenomenon was also observed in the oxidative scans. These results suggest an activation process of the Mg plating/stripping, which is attributed to an electrochemically inactive adsorption layer on the Mg surface and the nucleation process of crystalline Mg on the working electrode.<sup>12,18</sup> In sharp contrast, only comparatively small onset voltages of  $-0.17$  V and  $0.10$  V are necessary to start the initial plating/stripping of Mg in the electrolyte with 10 mM Bi(OTf)<sub>3</sub> additive. Furthermore, an enhanced reductive peak current of  $52 \text{ mA cm}^{-2}$  was recorded already in the first scan. After 10 cycles, the value stabilized at  $88 \text{ mA cm}^{-2}$  (**Figure 1c**). The initial Coulombic efficiency of the cell with additive is 92 % (**Figure 1d**), much higher than that of the cell without additive (83 %). The dip of the Coulombic efficiency for the pure electrolyte might be caused by the unstable

electrode/electrolyte interface (detailed explanation in Supporting Information), and it varies from cell to cell (**Figure S1**). However, they all showed lower Coulombic efficiencies than the additive-containing electrolyte. After 30 cycles, they became similar (**Figure S1**)

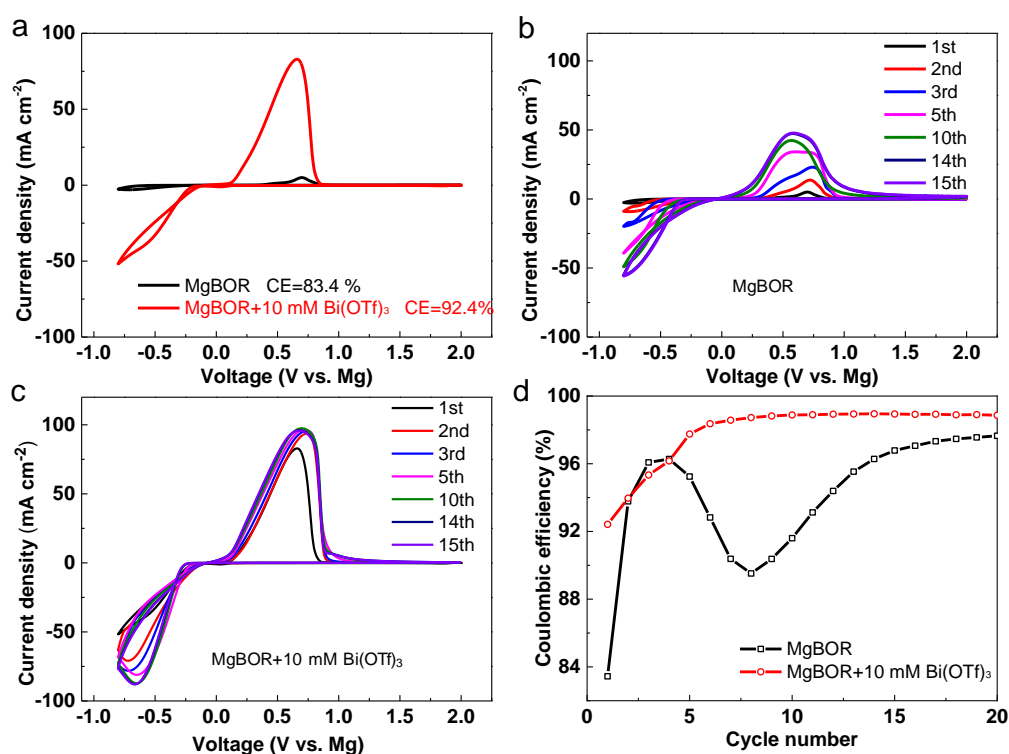


**Figure 1.** Cyclic voltammograms of MgBOR/DME electrolyte with and without  $\text{Bi}(\text{OTf})_3$  additive. (a) Comparison of the first cycle, (b, c) the first 15 cycles (b) without and (c) with additive, (d) comparison of the Coulombic efficiency.

The enhancement of Mg plating/stripping in the electrolyte with  $\text{Bi}(\text{OTf})_3$  is most probably caused by a change of the electrode/electrolyte interface. Due to the high standard potential of the  $\text{Bi}^{3+}/\text{Bi}$  (+ 0.308 V vs. SHE) couple, it is expected that  $\text{Bi}^{3+}$  could be reduced and deposit on the Mg surface spontaneously. In fact, the reduction

of a small amount of  $\text{Bi}(\text{OTf})_3$  on the working electrode surface at the onset of the first cathodic scan was also confirmed by **Figure S1**. The magnified CV curves revealed two additional peaks in the initial cathodic scan. The one centered at 1.8 V is supposed to be the formation of Bi on the work electrode surface. Another at 0.03 V in the first cycle and afterward shifted to around 0.2 V is related to the alloying process of Bi with Mg to form Mg-Bi alloy.<sup>32</sup> These Bi sediments on both the working electrode and Mg counter electrode act as nucleation sites to accelerate Mg deposition and reduce the adsorption layer on the Mg surface, leading to small plating/stripping overpotential.

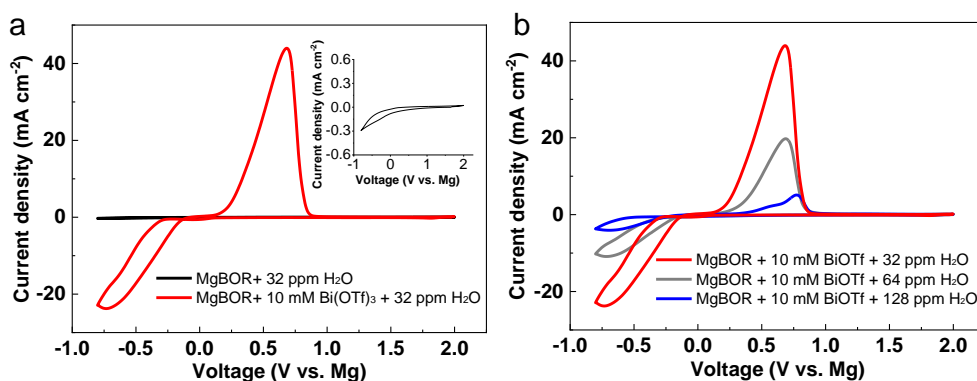


**Figure 2.** Cyclic voltammograms of (a) MgBOR/DME+32 ppm  $\text{H}_2\text{O}$  electrolyte with and without  $\text{Bi}(\text{OTf})_3$  additive (inset is the magnified CV of the black line), (b) MgBOR/DME+32ppm, 64 ppm and 128 ppm  $\text{H}_2\text{O}$  with  $\text{Bi}(\text{OTf})_3$  additive.

To further investigate the impact of  $\text{Bi}(\text{OTf})_3$  as an additive on Mg plating/stripping,  $\text{H}_2\text{O}$  was added deliberately to the electrolyte. As shown in **Figure 2a**, with the addition of 32 ppm of water into the blank electrolyte, no clear reduction/oxidation peaks related to Mg plating/stripping appeared anymore. Obviously, the additional

H<sub>2</sub>O leads to the formation of the MgO/Mg(OH)<sub>2</sub> passivation layer on the Mg surface, which impedes Mg<sup>2+</sup> ion diffusion.<sup>20,26</sup> This strong inhibiting role of H<sub>2</sub>O persisted in the following cycles with only a small amount of Mg plating/stripping (**Figure S2**) up to the 100th cycle, proving that the conditioning process scavenges H<sub>2</sub>O contaminant and removal of blocking layer is long. The electrolyte with Bi(OTf)<sub>3</sub> additive was also investigated with 32 ppm of H<sub>2</sub>O. The CV curves exhibited a remarkable plating/stripping process with a low plating overpotential of 0.22 V, a cathodic peak current of 25 mA cm<sup>-2</sup>, and Coulombic efficiency of 92 % in the initial cycle. It should be noted that an additional oxidative peak centered at 1.2 V was observed after prolonged cycling (Figure S2), which has been observed in some other Mg electrolyte systems. The origin of this peak is not yet clear.<sup>26,33</sup> When using the electrolyte with additive, further increasing the H<sub>2</sub>O concentration to 64 ppm and even 128 ppm did impede but not completely block the Mg plating/stripping process (**Figure 2b**).

In the next step, the influence of Bi(OTf)<sub>3</sub> additive on symmetric Mg/Mg cell performance was further tested by galvanostatic cycling. In the case of blank electrolyte, an immediate initial voltage spike to 2.9 V was observed at 1 mA cm<sup>-2</sup> during the on-off transition, followed by a high initial voltage polarization of 0.95 V (**Figure 3a**) between Mg plating/stripping. Consistent with the previous study, the high initial voltage spike and polarization are attributed to the adsorption layer of the electrochemical inactive species on the Mg anode surface.<sup>18</sup> The polarization voltage decreased successively in the subsequent cycles and reached a minimum of 0.14 V in the 78th cycle, indicating that the activation of the Mg/electrolyte interface is slow,

which is consistent with the CV result. When  $\text{Bi}(\text{OTf})_3$  was added to the electrolyte, both the initial voltage spike and Mg plating/stripping polarization in initial cycles decreased. This effect became more pronounced when increasing the concentration of  $\text{Bi}(\text{OTf})_3$ . The initial voltage spikes were drastically reduced to 2.1 V and 0.4 V with 2 mM and 10 mM  $\text{Bi}(\text{OTf})_3$  in the electrolyte, respectively, followed by a small plating/stripping polarization of 0.40 V and 0.21 V, respectively. It took only 37 cycles and 36 cycles for the cells with 2 mM and 10 mM  $\text{Bi}(\text{OTf})_3$  additive to reach their minimum Mg plating/stripping polarization voltage of 0.14 V, respectively (**Figure 3b**). Afterward, these three batteries exhibited only a little difference in Mg plating/stripping.

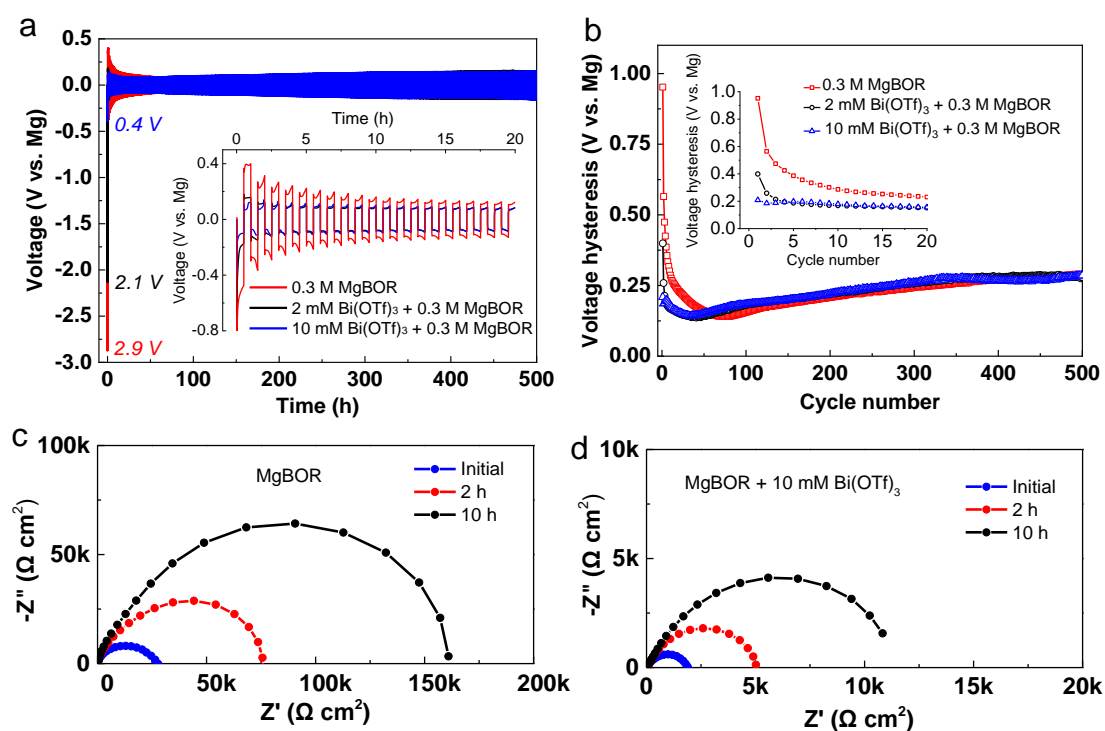


**Figure 3.** (a) Mg plating/stripping performance of the symmetric Mg/Mg cells in 0.3 M MgBOR/DME electrolyte with different concentrations of  $\text{Bi}(\text{OTf})_3$  at  $1 \text{ mA cm}^{-2}$ . (b) Corresponding voltage hysteresis of (a) (insets of (a) and (b) are the performance of the first 20 hours). (c and d) The

impedance of Mg/Mg cell after rest for different hours, (c) blank MgBOR/DME electrolyte, (d) MgBOR/DME electrolyte with 10 mM of Bi(OTf)<sub>3</sub>.

In the electrolyte, the electrochemical inactive species adsorbing on the Mg surface can greatly influence the interfacial resistance.<sup>18,34,35</sup> To monitor the differences in the interfacial conditions, electrochemical impedance spectra (EIS) of the symmetric Mg/Mg cells at different holding times and cyclings were recorded. Similar to prior studies,<sup>18,36</sup> large interfacial resistance of around 26 kΩ cm<sup>2</sup> in the fresh cell using pure MgBOR electrolyte at an open-circuit voltage (OCV) was recorded, which increased vastly with resting time (**Figure 3c**). After 10h rest, the interfacial impedance was as high as 163 kΩ cm<sup>2</sup> (208 kΩ, **Figure S3**, and **Table S1**). It is plausible that this high interfacial resistance is responsible for the high initial voltage spike in Figure 3a. The interfacial impedance in the cell with 10 mM Bi(OTf)<sub>3</sub> additive also increased with the rest time (**Figure 3d**). But it was only 12 kΩ cm<sup>2</sup> (15 kΩ, **Figure S3**, and **Table S1**) after resting for 10 h, showing an impressive decrease of more than one order of magnitude compared with the value of the pure electrolyte. The Nyquist plots of both cells exhibit analogous shape, indicating that the additive hadn't introduced any additional interfacial transport resistance.<sup>37</sup> When the cycling started, the impedance dropped dramatically in both cells (**Figure S4**). The cell with additive displayed impedance values of approximately 170 and 120 Ω cm<sup>2</sup> after 1 and 10 cycles, respectively, which are still smaller than the values of the cell without additive (approximately 1 kΩ cm<sup>2</sup> and 200 Ω cm<sup>2</sup> after 1 and 10 cycles, respectively). The lower interfacial impedance reveals fast charge transfer on the interface. After

150 cycles, the impedances of these two cells showed no evident difference and converged at  $50 \Omega \text{ cm}^2$  approximately.

### 3.2 Origin of the Beneficial Effects of $\text{Bi}(\text{OTf})_3$

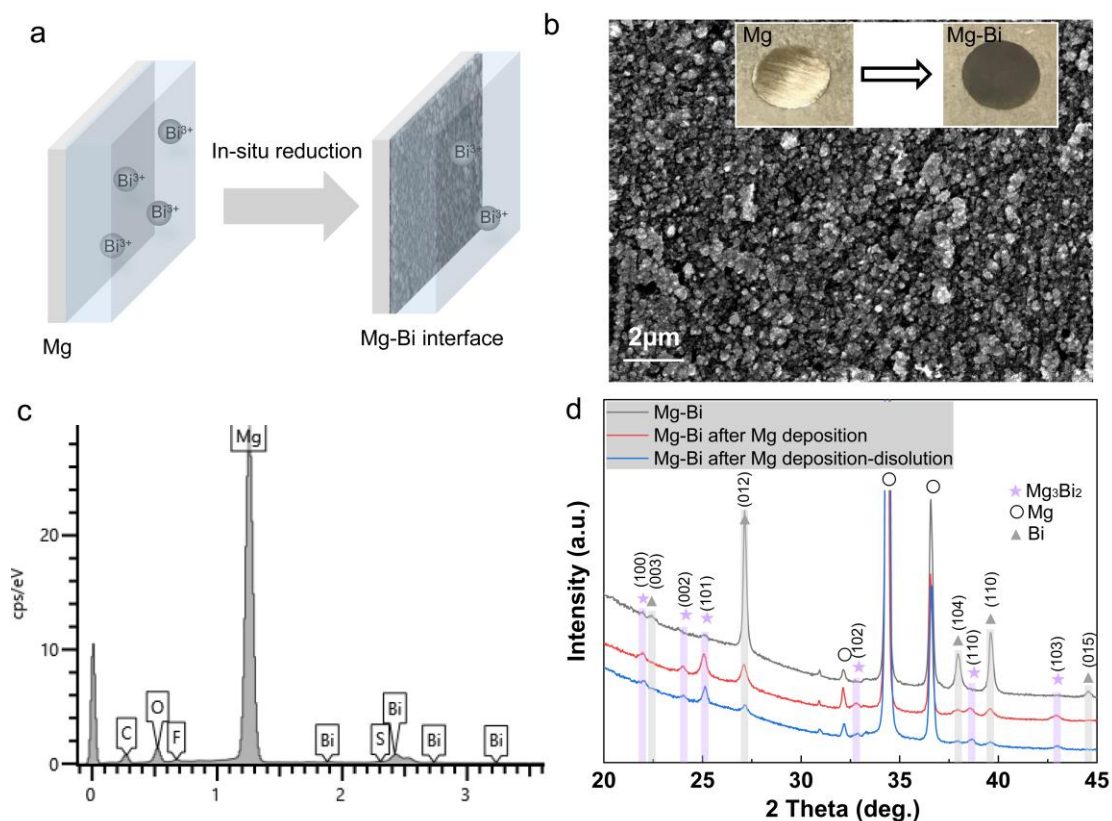


**Figure 4.** (a) Schematic illustration of the formation of Mg-Bi interface from  $\text{Bi}(\text{OTf})_3$  additive, (b) SEM image of Mg-Bi interface (inset shows the digital photos of Mg and Mg-Bi), (c) EDX element analysis of Mg-Bi interface, (d) ex-situ XRD of Mg-Bi at different charge/discharge state. Redline: Mg-Bi after  $1 \text{ mAh cm}^{-2}$  of Mg deposition (10 h at  $0.1 \text{ mA cm}^{-2}$ ). Blueline: Mg-Bi with  $1 \text{ mAh cm}^{-2}$  of Mg deposition followed by  $1 \text{ mAh cm}^{-2}$  of Mg dissolution (10 h at  $0.1 \text{ mA cm}^{-2}$ ).

The rational explanation for the lower interfacial resistance, the suppression of large initial voltage spike, and the smaller plating/stripping overpotential is that

Bi(OTf)<sub>3</sub> additive reacted with the Mg and *in-situ* deposits on the Mg surface (**Figure 4a**) to form a beneficial Mg-Bi interface. To prove this, a Mg electrode was exposed to 10 mM of Bi(OTf)<sub>3</sub>/DME solution for 10 s (denoted as Mg-Bi). The associated color change from silvery to black (**inset into Figure 4b**) gives the first indication for the evolution of the surface physical/chemical structures. Scanning electron microscopy (SEM) image of the pristine Mg anode showed a relatively smooth surface (**Figure S5**), while the treated Mg had a coarse morphology (**Figure 4b**). Bi signal appeared in the energy-dispersive X-ray spectroscopy (EDX) spectrum (**Figure 4c**), and the EDX mapping (**Figure S6**) showed that the Bi deposited on the Mg surface uniformly. The SEM image of the cross-section cut by focused ion beam (**Figure S7**) demonstrated the interface layer with a thickness of 200-300 nm composed of nanoparticles with an average size around 200 nm. Combined with the EDX mapping in Figure S6, we believe these nanoparticles are Bi-rich. The XPS measurements (**Figure S8**) corroborated the presence of Bi on the Mg surface in the Bi(OTf)<sub>3</sub>-containing electrolyte, which remained even after magnesium deposition or dissolution. It should be noted that it is difficult to distinguish between metallic and alloyed Bi since the chemical shift is small in this case.<sup>38-40</sup> The Mg 2p spectra (**Figure S9**) could be fitted with two peaks at 49.4 and 50.9 eV, which are assigned to metallic Mg<sup>0</sup> and various Mg<sup>2+</sup>-containing compounds (like MgO, Mg(OH)<sub>2</sub>, MgF<sub>2</sub>, or Mg<sub>3</sub>Bi<sub>2</sub>).<sup>16,29</sup> The F 1s spectrum showed two split peaks at 685.7 and 688.6 eV, respectively, corresponding to MgF<sub>2</sub> and -CF<sub>3</sub>. The latter comes from the electrolyte residues. The O 1s spectrum could be fitted into three peaks at 530.4 (C-O), 531.7

(C=O and/or Mg(OH)<sub>2</sub>), and 533.5 (MgO) eV. The XPS spectra indicated that apart from the Bi-containing species, the interface might also contain some non-Mg<sup>2+</sup> ion-conducting composites, such as MgF<sub>2</sub>, MgO, and Mg (OH)<sub>2</sub>. X-ray diffraction (XRD) was carried out to identify the composition of the interphase further. To get a clear XRD pattern, DME containing 100 mM of Bi(OTf)<sub>3</sub> was used to prepare a dense Mg-Bi interface (see details in Experiment Section). As shown in **Figure 4d**, in addition to the signals of Mg metal, reflections at 27.2, 38.0, 39.6, 44.6, 46.0, and 48.7° were observed (gray line), indicating that metallic Bi with R-3m space group was formed on the Mg surface. In addition, Mg<sub>3</sub>Bi<sub>2</sub> alloy formation was also observed (**Figure S10**), which is evidenced by the reflections labeled with asterisks (21.9, 24.0, and 25.1°, corresponding to (100) (002) and (101), respectively). Two other Mg-Bi electrodes were characterized after Mg deposition and dissolution (Figure 4d) to further clarify the Bi-consisting interface evolution during Mg plating/stripping. After Mg deposition and dissolution, the signals of Bi became weak, and the intensities of the Mg<sub>3</sub>Bi<sub>2</sub> phase increased, suggesting that most of the Bi converted to Mg<sub>3</sub>Bi<sub>2</sub> on the Mg surface during the electrochemical process.

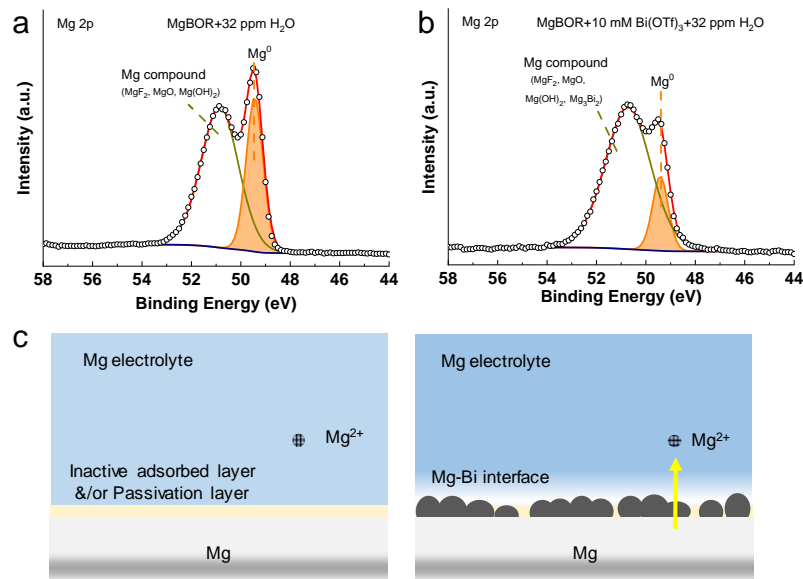


Figure 5. Mg 2p XPS spectra of the Mg electrode after exposure to different electrolytes for 5h, (a) MgBOR/DME+32 ppm H<sub>2</sub>O electrolyte, (b) MgBOR/DME+10 mM Bi(OTf)<sub>3</sub>+32 ppm H<sub>2</sub>O electrolyte, (c) schematic illustration of the role of in-situ formed Mg-Bi interface.

XPS was also used to study possible changes of the Mg electrode after contacting with a water-containing (32 ppm H<sub>2</sub>O) electrolyte (**Figure 5a and b**). The decrease of the relative intensity of the Mg<sup>0</sup> peak for the Mg-Bi sample suggests that the (metallic) Mg substrate was buried below a thicker layer here. This can be explained at least in part by forming the Bi-containing layer, which covered the surface. In addition to the Mg compound, the peaks of C-O, C=O, and -CF<sub>3</sub> were also observed (**Figure S11**), which may primarily come from the electrolyte residues.

Compared with the pure Mg surface, it is more difficult to form an effective passivation layer on the Mg-Bi surface.<sup>29</sup> Obviously, the *in-situ* deposited Bi/Mg<sub>3</sub>Bi<sub>2</sub> on the Mg surface leads to less exposure of the highly reactive Mg surface to the electrolyte, which reduces the electrochemical inactive species adsorbing on the

electrode surface (**Figure 5c**). Importantly,  $\text{Mg}^{2+}$  ion mobility in  $\text{Mg}_3\text{Bi}_2$  is relatively fast ( $\sim 10^{-10} \text{ cm}^2 \text{ s}^{-1}$ , migration barrier of 0.30-0.41 eV)<sup>29-31</sup> compared with the adsorbed electrochemical inactive species and the passivation layer (e.g., the migration barrier in  $\text{MgO}$  is 1.86 eV).<sup>41</sup> This multi-functional interphase increases the active sites for Mg plating/stripping and facilitates  $\text{Mg}^{2+}$  ion transfer between the liquid and the solid phase. As a result, the large interfacial impedances at both static and dynamic conditions are largely reduced, leading to a significant drop of voltage spike during the on-off transition and low overpotentials in the first dozens of cycles. The original surface morphology changed enormously with inhomogeneous elemental Bi distribution after multiple Mg plating/stripping cycles at  $1 \text{ mA cm}^{-2}$ . Meanwhile, the Mg metal could be detected on the surface (**Figure S12 and S13**), implying Mg plating/stripping could eventually override the Mg-Bi layer under  $1 \text{ mA cm}^{-2}$ . After 100 cycles in  $50 \mu\text{L MgBOR/DME} + 10 \text{ mM Bi(OTf)}_3$  electrolyte (**Figure S14**), the  $\text{Mg}_3\text{Bi}_2$  XRD pattern was undetectable, which may be caused by two reasons: 1) the electrochemical grinding reduced the particle size<sup>32</sup> and/or the crystallinity of  $\text{Mg}_3\text{Bi}_2$ , 2) the  $\text{Mg}_3\text{Bi}_2$  was covered by Mg.

During cycling, the  $\text{Bi}^{3+}$  would be consumed, and ultimately, the pure Mg metal was exposed to the electrolyte, which was passivated by the impurities ( $\text{H}_2\text{O}$ ,  $\text{O}_2$ , and  $\text{CO}_2$ ) and the  $\text{MgF}_2$ . That is why after multiple cycles, the  $\text{Bi(OTf)}_3$  additive lost its beneficial effect. The EIS spectra in Figure S5 also indicate the degradation of the interface. The Mg/Mg cell using MgBOR/DME electrolyte with 10 mM of  $\text{Bi(OTf)}_3$  exhibited a minimum of  $36 \Omega \text{ cm}^2$ . After that, the impedance increased a little bit until

a stable value of  $50 \Omega \text{ cm}^2$ . The increase of the impedance may be ascribed to the degradation of the interface. This is the probable reason for the similar electrochemical performance of the electrolytes with and without the additive after multiple cycles. The advantage of the  $\text{Bi}(\text{OTf})_3$  additive is that the initial large overpotentials could be avoided. In Mg battery systems, Mg anode is highly sensitive to the impurities in the electrolyte (e.g.,  $\text{H}_2\text{O}$ ,  $\text{O}_2$ ,  $\text{CO}_2$ , etc.), which will passivate the Mg surface. The passivation is more prominent with the existence of water, as shown in Figure 2. However, these impurities are inevitable, especially in the large-scale preparation of the electrolyte. The electrolyte conditioning could remove the impurities,<sup>42,43,44</sup> but it is time-consuming and expensive. The additive plays a role of a “trigger” that induces high reversible Mg plating/stripping initially, rendering conditioning of the electrolyte unnecessary.

In practical operation, the large Mg anode overpotential in initial cycles will be undoubtedly reflected in the entire cell performance, which had been proved by three-electrode cells with chevrel phase  $\text{Mo}_6\text{S}_8$  cathodes (**Figure S15**). This impact became stronger at a higher current density (**Figure S16**). Compared with the Mg anode, the Mg-Bi interface ensured a smaller overpotential of the full cell. High cathode active material loading and high current density are inevitable for practical Mg batteries to achieve high energy density and high power. Both of them will lead to the increase of current density on the Mg anode side. As a result, proper regulation of the Mg anode/electrolyte interface, e.g., by establishing functional interphase as presented in this study, can be an effective way to enabling an improved operation of

the full cells. It should be noted that during the battery operation, we found that not only the Mg anode but also the Mo<sub>6</sub>S<sub>8</sub> cathode suffered from an “activation” process. However, the mechanism of this “cathode activation” is beyond the scope of this article.

A recent report has shown that the anion association strength in the electrolyte could systematically influence the overpotential for metal stripping/plating. In the study, OTf<sup>-</sup> anion could lower the dissolution overpotential of Zn.<sup>45</sup> To investigate the effect of the OTf<sup>-</sup> anion on the solvation structure, Raman analysis was used (**Figure S17**). The characteristic peak at 880 cm<sup>-1</sup> of the electrolyte associated with the symmetric breathing mode of the three DME molecules encaging Mg<sup>2+</sup> ions to form Mg<sup>2+</sup>DME<sub>3</sub> solvated cations,<sup>46,47</sup> which didn't change after the addition of 10 mM Bi(OTf)<sub>3</sub>, indicating the solvation structure is not affected. To further confirm the Bi rendered smaller Mg deposition/dissolution polarization, rather than OTf<sup>-</sup> anion, the Mg-Bi electrode prepared from 10 mM of Bi(OTf)<sub>3</sub>/DME electrolyte (Experimental Section) was chosen for symmetrical cell test. A blank electrolyte was used in this case. The identical electrochemical performances of the symmetric Mg-Bi/Mg-Bi cell (**Figure S18**) to the Mg/Mg cell with 10 mM Bi(OTf)<sub>3</sub> additive (Figure 3) at 1mA cm<sup>-2</sup> suggests that Bi/Mg<sub>3</sub>Bi<sub>2</sub> on the Mg surface is responsible for the superior performance.

#### 4. CONCLUSIONS

In summary, Bi(OTf)<sub>3</sub> was examined as a new additive for Mg electrolytes. It drastically reduces the initial voltage spike and the overpotential for Mg

plating/stripping in the following dozens of cycles in the MgBOR/DME electrolyte. The additive-containing electrolyte even exhibits tolerance to water impurities as high as 128 ppm. These beneficial results are attributed to the in-situ formed Bi/Mg<sub>3</sub>Bi<sub>2</sub> interface on the Mg anode surface. The Bi-based functional interphase could suppress the adsorption of electrochemical inactive species on the Mg surface and alleviate surface passivation. As a result, efficient charge transfer during the on-off transition and the initial dozens of cycles is guaranteed, enabling a conditioning-free Mg plating/stripping process.

## **ASSOCIATED CONTENT**

Supporting information

Cyclic voltammograms, EIS, SEM, EDS, XRD, and XPS measurements of the electrode, Raman spectra of the electrolytes, electrochemical performance of symmetric Mg/Mg, Mg-Bi/Mg-Bi cells, and Mo<sub>6</sub>S<sub>8</sub>/Mg cell.

## **AUTHOR INFORMATION**

### **Corresponding Author:**

\*E-mail:

zhen.meng@partner.kit.edu

zhirong.zhao-karger@kit.edu

maximilian.fichtner@kit.edu

## **Notes**

The authors declare no competing financial interest.

## ACKNOWLEDGEMENTS

This work contributes to the research performed at CELEST (Center for Electrochemical Energy Storage Ulm-Karlsruhe) and was funded by the German Research Foundation (DFG) under Project ID 390874152 (POLiS Cluster of Excellence).

## REFERENCES

- (1) Gregory, T. D.; Hoffman, R. J.; Winterton, R. C. Nonaqueous Electrochemistry of Magnesium: Applications to Energy Storage. *J. Electrochem. Soc.* **1990**, *137*, 775–780.
- (2) Liang, Y.; Dong, H.; Aurbach, D.; Yao, Y. Current Status and Future Directions of Multivalent Metal-Ion Batteries. *Nat. Energy* **2020**, *5*, 646–656.
- (3) Kim, H. S.; Arthur, T. S.; Allred, G. D.; Zajicek, J.; Newman, J. G.; Rodnyansky, A. E.; Oliver, A. G.; Boggess, W. C.; Muldoon, J. Structure and Compatibility of a Magnesium Electrolyte with a Sulphur Cathode. *Nat. Commun.* **2011**, *2*, 427–432.
- (4) Xu, X.; Chao, D.; Chen, B.; Liang, P.; Li, H.; Xie, F.; Davey, K.; Qiao, S.-Z. Revealing the Magnesium-Storage Mechanism in Mesoporous Bismuth via Spectroscopy and Ab-Initio Simulations. *Angew. Chemie Int. Ed.* **2020**, *59*, 21728–21735.
- (5) Aurbach, D.; Lu, Z.; Schechter, A.; Gofer, Y.; Gizbar, H.; Turgeman, R.; Cohen, Y.; Moshkovich, M.; Levi, E. Prototype Systems for Rechargeable Magnesium

- Batteries. *Nature* **2000**, *407*, 724–727.
- (6) Zhao-Karger, Z.; Zhao, X.; Wang, D.; Diemant, T.; Behm, R. J.; Fichtner, M. Performance Improvement of Magnesium Sulfur Batteries with Modified Non-Nucleophilic Electrolytes. *Adv. Energy Mater.* **2015**, *5*, 1401155.
- (7) Tutusaus, O.; Mohtadi, R.; Arthur, T. S.; Mizuno, F.; Nelson, E. G.; Sevryugina, Y. V. An Efficient Halogen-Free Electrolyte for Use in Rechargeable Magnesium Batteries. *Angew. Chemie Int. Ed.* **2015**, *54*, 7900–7904.
- (8) Shterenberg, I.; Salama, M.; Yoo, H. D.; Gofer, Y.; Park, J.-B.; Sun, Y.-K.; Aurbach, D. Evaluation of  $(\text{CF}_3\text{SO}_2)_2\text{N}-(\text{TFSI})$  Based Electrolyte Solutions for Mg Batteries. *J. Electrochem. Soc.* **2015**, *162*, A7118–A7128.
- (9) Hahn, N. T.; Seguin, T. J.; Lau, K.-C.; Liao, C.; Ingram, B. J.; Persson, K. A.; Zavadil, K. R. Enhanced Stability of the Carba-Closo-Dodecaborate Anion for High-Voltage Battery Electrolytes through Rational Design. *J. Am. Chem. Soc.* **2018**, *140*, 11076–11084.
- (10) Herb, J. T.; Nist-Lund, C. A.; Arnold, C. B. A Fluorinated Alkoxyaluminate Electrolyte for Magnesium-Ion Batteries. *ACS Energy Lett.* **2016**, *1*, 1227–1232.
- (11) Luo, J.; Bi, Y.; Zhang, L.; Zhang, X.; Liu, T. L. A Stable, Non-Corrosive Perfluorinated Pinacolatoborate Mg Electrolyte for Rechargeable Mg Batteries. *Angew. Chemie Int. Ed.* **2019**, *58*, 6967–6971.
- (12) Zhao-Karger, Z.; Gil Bardaji, M. E.; Fuhr, O.; Fichtner, M. A New Class of Non-Corrosive, Highly Efficient Electrolytes for Rechargeable Magnesium

- Batteries. *J. Mater. Chem. A* **2017**, *5*, 10815–10820.
- (13) Ran A.; Michael S.; Baruch H.; Yosef G.; Doron A. Anode-Electrolyte Interfaces in Secondary Magnesium Batteries. *Joule* **2019**, *3*, 27–56.
- (14) Salama, M.; Attias, R.; Hirsch, B.; Yemini, R.; Gofer, Y.; Noked, M.; Aurbach, D. On the Feasibility of Practical Mg–S Batteries: Practical Limitations Associated with Metallic Magnesium Anodes. *ACS Appl. Mater. Interfaces* **2018**, *10*, 36910–36917.
- (15) Li, X.; Gao, T.; Han, F.; Ma, Z.; Fan, X.; Hou, S.; Eidson, N.; Li, W.; Wang, C. Reducing Mg Anode Overpotential via Ion Conductive Surface Layer Formation by Iodine Additive. *Adv. Energy Mater.* **2018**, *8*, 1701728.
- (16) Gao, T.; Hou, S.; Huynh, K.; Wang, F.; Eidson, N.; Fan, X.; Han, F.; Luo, C.; Mao, M.; Li, X.; Wang, C. Existence of Solid Electrolyte Interphase in Mg Batteries: Mg/S Chemistry as an Example. *ACS Appl. Mater. Interfaces* **2018**, *10*, 14767–14776.
- (17) Aurbach, D.; Schechter, A.; Moshkovich, M.; Cohen, Y. On the Mechanisms of Reversible Magnesium Deposition Processes. *J. Electrochem. Soc.* **2001**, *148*, A1004–A1014.
- (18) Tutusaus, O.; Mohtadi, R.; Singh, N.; S. Arthur, T.; Mizuno, F. Study of Electrochemical Phenomena Observed at the Mg Metal/Electrolyte Interface. *ACS Energy Lett.* **2016**, *2*, 224–229.
- (19) Shterenberg, I.; Salama, M.; Gofer, Y.; Levi, E.; Aurbach, D. The Challenge of Developing Rechargeable Magnesium Batteries. *MRS Bull.* **2014**, *39*, 453–460.

- (20) Shterenberg, I.; Salama, M.; Yoo, H. D.; Gofer, Y.; Park, J.-B.; Sun, Y.-K.; Aurbach, D. Evaluation of  $(\text{CF}_3\text{SO}_2)_2\text{N}-(\text{TFSI})$  Based Electrolyte Solutions for Mg Batteries. *J. Electrochem. Soc.* **2015**, *162*, A7118–A7128.
- (21) Son, S.-B.; Gao, T.; Harvey, S. P.; Steirer, K. X.; Stokes, A.; Norman, A.; Wang, C.; Cresce, A.; Xu, K.; Ban, C. An Artificial Interphase Enables Reversible Magnesium Chemistry in Carbonate Electrolytes. *Nat. Chem* **2018**, *10*, 532–539.
- (22) Tang, K.; Du, A.; Dong, S.; Cui, Z.; Liu, X.; Lu, C.; Zhao, J.; Zhou, X.; Cui, G. A Stable Solid Electrolyte Interphase for Magnesium Metal Anode Evolved from a Bulky Anion Lithium Salt. *Adv. Mater.* **2019**, *32*, 1904987.
- (23) Zhang, J.; Guan, X.; Lv, R.; Wang, D.; Liu, P.; Luo, J. Rechargeable Mg Metal Batteries Enabled by a Protection Layer Formed in Vivo. *Energy Storage Mater.* **2020**, *26*, 408–413.
- (24) Lv, R.; Guan, X.; Zhang, J.; Xia, Y.; Luo, J. Enabling Mg Metal Anodes Rechargeable in Conventional Electrolytes by Fast Ionic Transport Interphase. *Natl. Sci. Rev.* **2020**, *7*, 333–341.
- (25) Sa, N.; Pan, B.; Saha-Shah, A.; Hubaud, A. A.; Vaughey, J. T.; Baker, L. A.; Liao, C.; Burrell, A. K. Role of Chloride for a Simple, Non-Grignard Mg Electrolyte in Ether-Based Solvents. *ACS Appl. Mater. Interfaces* **2016**, *8*, 16002–16008.
- (26) Connell, J. G.; Genorio, B.; Lopes, P. P.; Strmcnik, D.; Stamenkovic, V. R.; Markovic, N. M. Tuning the Reversibility of Mg Anodes via Controlled

- Surface Passivation by  $\text{H}_2\text{O}/\text{Cl}^-$  in Organic Electrolytes. *Chem. Mater.* **2016**, *28*, 8268–8277.
- (27) Salama, M.; Shterenberg, I.; Shimon, L. J. W.; Keinan-Adamsky, K.; Afri, M.; Gofer, Y.; Aurbach, D. Structural Analysis of Magnesium Chloride Complexes in Dimethoxyethane Solutions in the Context of Mg Batteries Research. *J. Phys. Chem. C* **2017**, *121*, 24909–24918.
- (28) Attias, R.; Salama, M.; Hirsch, B.; Goffer, Y.; Aurbach, D. Anode-Electrolyte Interfaces in Secondary Magnesium Batteries. *Joule* **2019**, *3*, 27–52.
- (29) Matsui, M.; Kuwata, H.; Mori, D.; Imanishi, N.; Mizuhata, M. Destabilized Passivation Layer on Magnesium-Based Intermetallics as Potential Anode Active Materials for Magnesium Ion Batteries. *Front. Chem* **2019**, *7*, 7.
- (30) Jung, S. C.; Han, Y.-K. Fast Magnesium Ion Transport in the  $\text{Bi}/\text{Mg}_3\text{Bi}_2$  Two-Phase Electrode. *J. Phys. Chem. C* **2018**, *122*, 17643–17649.
- (31) Lee, J.; Monserrat, B.; Seymour, I. D.; Liu, Z.; Dutton, S. E.; Grey, C. P. An Ab Initio Investigation on the Electronic Structure, Defect Energetics, and Magnesium Kinetics in  $\text{Mg}_3\text{Bi}_2$ . *J. Mater. Chem. A* **2018**, *6*, 16983–16991.
- (32) Murgia, F.; Stievano, L.; Monconduit, L.; Berthelot, R. Insight into the Electrochemical Behavior of Micrometric Bi and  $\text{Mg}_3\text{Bi}_2$  as High Performance Negative Electrodes for Mg Batteries. *J. Mater. Chem. A* **2015**, *3*, 16478–16485.
- (33) Kim, S. S.; Bevilacqua, S. C.; See, K. A. Conditioning-Free Mg Electrolyte by the Minor Addition of  $\text{Mg}(\text{HMDS})_2$ . *ACS Appl. Mater. Interfaces* **2020**, *12*,

- 5226–5233.
- (34) Aurbach, D. Magnesium Deposition and Dissolution Processes in Ethereal Grignard Salt Solutions Using Simultaneous EQCM-EIS and In Situ FTIR Spectroscopy. *Electrochem. Solid-State Lett.* **1999**, *3*, 31–34.
- (35) Mizuno, F.; Singh, N.; Arthur, T. S.; Fanson, P. T.; Ramanathan, M.; Benmayza, A.; Prakash, J.; Liu, Y.-S.; Glans, P.-A.; Guo, J. Understanding and Overcoming the Challenges Posed by Electrode/Electrolyte Interfaces in Rechargeable Magnesium Batteries. *Front. Energy Res.* 2014, *2*, 46.
- (36) Zhao-Karger, Z.; Liu, R.; Dai, W.; Li, Z.; Diemant, T.; Vinayan, B. P.; Bonatto Minella, C.; Yu, X.; Manthiram, A.; Behm, R. J.; Ruben, M.; Fichtner M. Toward Highly Reversible Magnesium–Sulfur Batteries with Efficient and Practical Mg[B(Hfip)<sub>4</sub>]<sub>2</sub> Electrolyte. *ACS Energy Lett.* **2018**, *3*, 2005–2013.
- (37) Tu, Z.; Choudhury, S.; Zachman, M. J.; Wei, S.; Zhang, K.; Kourkoutis, L. F.; Archer, L. A. Fast Ion Transport at Solid–solid Interfaces in Hybrid Battery Anodes. *Nat. Energy* **2018**, *3*, 310–316.
- (38) Ren, Y. X.; Zeng, L.; Jiang, H. R.; Ruan, W. Q.; Chen, Q.; Zhao, T. S. Rational Design of Spontaneous Reactions for Protecting Porous Lithium Electrodes in Lithium–sulfur Batteries. *Nat. Commun.* **2019**, *10*, 3249–3258.
- (39) Zhou, G.-T.; Palchik, O.; Pol, V. G.; Sominski, E.; Koltypin, Y.; Gedanken, A. Microwave-Assisted Solid-State Synthesis and Characterization of Intermetallic Compounds of Li<sub>3</sub>Bi and Li<sub>3</sub>Sb. *J. Mater. Chem.* **2003**, *13*, 2607–2611.

- (40) Moulder, J. F.; Stickle, W. F.; Sobol, P. E.; Bomben, K. D. Handbook of X Ray Photoelectron Spectroscopy: A Reference Book of Standard Spectra for Identification and Interpretation of XPS Data. *Physical Electronics, Reissue edition*. **1995**, ISBN: 096481241X, 189–190.
- (41) Chen, T.; Sai Gautam, G.; Canepa, P. Ionic Transport in Potential Coating Materials for Mg Batteries. *Chem. Mater.* **2019**, *31*, 8087–8099.
- (42) Barile, C. J.; Barile, E. C.; Zavadil, K. R.; Nuzzo, R. G.; Gewirth, A. A. Electrolytic Conditioning of a Magnesium Aluminum Chloride Complex for Reversible Magnesium Deposition. *J. Phys. Chem. C* **2014**, *118*, 27623–27630.
- (43) Fukutsuka, T.; Asaka, K.; Inoo, A.; Yasui, R.; Miyazaki, K.; Abe, T.; Nishio, K.; Uchimoto, Y. New Magnesium-Ion Conductive Electrolyte Solution Based on Triglyme for Reversible Magnesium Metal Deposition and Dissolution at Ambient Temperature. *Chem. Lett.* **2014**, *43*, 1788–1790.
- (44) Kang, S.-J.; Lim, S.-C.; Kim, H.; Heo, J. W.; Hwang, S.; Jang, M.; Yang, D.; Hong, S.-T.; Lee, H. Non-Grignard and Lewis Acid-Free Sulfone Electrolytes for Rechargeable Magnesium Batteries. *Chem. Mater.* **2017**, *29*, 3174–3180.
- (45) Connell, J. G.; Zorko, M.; Agarwal, G.; Yang, M.; Liao, C.; Assary, R. S.; Strmcnik, D.; Markovic, N. M. Anion Association Strength as a Unifying Descriptor for the Reversibility of Divalent Metal Deposition in Nonaqueous Electrolytes. *ACS Appl. Mater. Interfaces* **2020**, *12*, 36137–36147.
- (46) Attias, R.; Salama, M.; Hirsch, B.; Gofer, Y.; Aurbach, D. Solvent Effects on the Reversible Intercalation of Magnesium-Ions into V<sub>2</sub>O<sub>5</sub> Electrodes.

*ChemElectroChem* **2018**, *5*, 3514–3524.

- (47) Salama, M.; Shterenberg, I.; Gizbar, H.; Eliaz, N. N.; Kosa, M.; Keinan-Adamsky, K.; Afri, M.; Shimon, L. J. W.; Gottlieb, H. E.; Major, D. T.; Yosef Gofer, Y.; Aurbach, D. Unique Behavior of Dimethoxyethane (DME)/Mg(N(SO<sub>2</sub>CF<sub>3</sub>)<sub>2</sub>)<sub>2</sub> Solutions. *J. Phys. Chem. C* **2016**, *120*, 19586–19594.

For Table of Content only

